



Body Impedance Spectroscopy Based on Electrical Relaxation Behavior: Advantages and Challenges

Uwe Pliquet^a, Nguyen Ngoc Duc^b, Trinh Dinh Yen^b,
Nguyen Thi Thuong^b, and Le Manh Hai^b

^aInstitut für Bioprozess- und Analysenmesstechnik, Heilbad Heiligenstadt, Germany

^bInstitute of Biomedical Physics, Ho Chi Minh City, Viet Nam

Correspondence: Uwe Pliquet, Institut für Bioprozess- und Analysenmesstechnik e.V., 37308 Heilbad Heiligenstadt, Germany
E-mail: uwe.pliquet@iba-heiligenstadt.de Website: www.iba-heiligenstadt.de Phone: +49 37308 671315

Abstract. The body impedance analysis (BIA) is, although not always sufficiently selective, a well-recognized tool for easy assessment of body composition. Compared to the sole measurement of the impedance magnitude at one frequency (e.g., 50 kHz), the complex impedance over a frequency range provides additional information, especially about the body composition. Other than impedance spectroscopy in the frequency domain, time domain based methods offer fast measurement with high repetition rate using affordable instrumentation.

Although the instrumentation is very easy to accomplish, high reproducibility of the results, as well as extraction of behavior significantly linked to body state, needs basic knowledge of factors influencing the electrical behavior between the electrodes like for instance parasitic capacities. Moreover, not all stimulation signals behave in the same way, either they are complicated to synthesize, or they are sensitive to uncertainties in the measurement chain. Although multisine stimulation is simple and stable, it lacks the potential for a minimalistic approach. Here we show a way of processing the response to a step function as a basis for future hardware developments. The system presented here assesses the electrical properties in a frequency range between 100 Hz and 1 MHz within 10 ms. Although simple processing using fast Fourier transformation is feasible, we show a signal processing on the basis of adaptive sampling which is compatible with future developments of broad bandwidth, high-speed systems with low data volume and extremely low power consumption.

Keywords: body impedance spectroscopy, electric relaxation, body composition, data processing

1. Introduction

Body composition is an important measure, not only for bodybuilding or cosmetics but mostly for a medical reason. The body composition, here overwhelmingly the fat content and hydration state, can guide rehabilitation therapy but is also used for estimation of risks for patients undergoing surgery or any kind of analgesia.

The use of electrical impedance measurement relies on the fact that different tissues can be discriminated by their electrical impedance (Gabriel et al. 1996, Schwan 1957, Schwan 1993, McAdams et al. 1995). Blood has higher conductivity (1.4 S/m) than muscle (0.4 S/m perpendicular, 0.85 S/m longitudinal to the fibers) and tissues like fat (0.02 S/m) and bone (0.015 S/m) show low conductivity. Even less conductive would be air (10^{-8} S/m) inside the inflated lungs.

Modeling the body seems at first glance fairly simple since the geometry of an average body, and the electrical behavior of tissues are known. However, with only a few variables measured, it is not possible to assess the elements of a complicated model. If for instance only the magnitude of the impedance at a single frequency is measured, only a very simple model can be calculated (de Lorenzo et al. 1991).

With phase information, additional information about compartments surrounded by insulating cell membranes becomes feasible which allows the distinction between water in- and outside of cells. Unfortunately, this is not sufficient for assessment of the fraction of free body water (i.e., inside intestine) and water bound in tissues. Having information on electrical properties over a higher frequency range can considerably increase the significance of the derived properties (Hannan 1995, Cornish 1996).

Today, the general approach for impedance spectroscopy at whole body uses a sweep through the interesting frequency range and measurement of the impedance magnitude and phase at each frequency (frequency domain) (Cornish 1996). This takes time, up to more than a minute depending on selected frequencies and integration time at each frequency. A great uncertainty arises from moving artifacts and body functions like respiration or heartbeat. This can be overcome by fast measurements, at least twice faster than the period of such periodic events. Else, at least three measurements are necessary in order to rule out false results.

Fast measurements in the time domain are common in several fields of bioimpedance measurement, but most commercial BIA-devices do not use this approach. Several studies using broad bandwidth excitation with monitoring the response in the time domain are reported, mostly by employing multisine signals (Bragos 2001, Min, 2008). In general, after Fourier transformation of these signals further processing is done in the frequency domain. Although step function or square wave (voltage or current controlled) as stimulus (Lykken 1971) is employed as well, it is often rejected by most researchers due to the following reasons:

1. If equidistant sampling of the time function with subsequent Fourier transformation is used, high-level noise appears at high frequencies due to the low energy of the higher harmonics.
2. The use of broad bandwidth amplifiers does not allow efficient noise reduction as it is possible with lock-in amplifiers at single frequency measurements.
3. The reproducibility, especially in the high-frequency range is often poor due to the jitter of low-cost acquisition systems (simple digital oscilloscope) where the channels are not synchronously triggered.
4. The use of low-resolution analog-to-digital-converters (ADC) (e.g., 8-bit) results in uncertainties at low frequency (quantization noise).
5. Although well known, signals are often not consequently preprocessed, which results in higher quantization noise (e.g. only 6 or 7 bit used because the signal is too small) or aliasing effects (insufficient filtering).

However, all these limitations based on the practical approach but they are theoretically irrelevant, if the signals are processed in a proper way.

When seeking fast methods with minimal energy consumption, employing step response is an excellent choice (Pliquett 2000). This, however, needs a more sophisticated approach than equidistant sampling with 8-bit resolution. A good approach may include:

1. If equidistant sampling is preferred due to the availability of the instrumentation (IO-cards, digital oscilloscope, data acquisition system) at least 12-bit resolution should be used. Moreover, the jitter between signal generation and sampling should be minimized. This does not only regard the instruments like arbitrary function generators but also the mostly homemade frontends and cabling.
2. A transformation into the frequency domain is not necessary. Since the response of typical biological tissue to step functions (current or voltage) is the sum of exponentials, a direct calculation in time domain resulting in relaxation times and relaxation strengths (relaxation spectroscopy) is much faster and yields comparable information. If needed, a simple calculation yields the impedance spectrum. Critical in this approach is the quality of the excitation signal. The step should be clear without overshoot, and the rest of the signal has to be as flat as possible. Else, the measurement precision is comprised, or more complicated calculations are required.
3. The highest frequency components appear immediately after the step while later only low-frequency compounds are found. Therefore, a high sampling rate is necessary at the beginning of the signal and can be significantly less, by orders of magnitude, while the excitation signal lasts. It should be noted, that an anti-aliasing filter should be adapted to the sampling rate in order to avoid unrecognized errors in the sampled signal.

Although some effort seems unavoidable, this approach shows important features for upcoming applications.

If a broad bandwidth signal (multisine, chirp, step response) is sampled in order to achieve a frequency range of for instance four orders of magnitude (e.g., 100 Hz (f_{low}) – 1 MHz (f_{high})), according to the sampling theorem at least 20.000 samples ($N_{samples, min}$) are necessary:

$$N_{samples, min} = 2 \cdot f_{high} / f_{low} \quad (1)$$

With adaptive sampling, it can be reduced to 4 – 10 samples per decade, where six samples per decade yield typically sufficiently good results. This means, in the aforementioned example (4 orders of magnitude) only 24 samples are needed. This has two important advantages: (1) Because of the low number of samples, the ADC can be slow, but high resolution (e.g., 16 bit) and (2) the data stream is sufficiently low which allows continuous monitoring. A serious problem arises from the violation of Kotelnikov's sampling theorem which increases with longer times between the sampling points. In order to create an adaptive anti-aliasing filter, the signal should be integrated between two sampling times. This approach, however, needs special hardware for generation of the sampling times and signal integration.

To show the feasibility but also problems associated with this approach, we used a continuous sampling system (oscilloscope) but process the data in a way as it would have been after partial integration with adaptive sampling. Moreover, we used multisine measurements as a control. This allowed testing critical parameters for future developments of sophisticated hardware.

2. Materials and Methods

2.1 Electrodes

Commercial ECG-electrodes from two different manufacturers were used throughout the experiments. Since the Ag/AgCl-electrodes F-TB1 (skintact®, Leonard Lang GmbH, Austria) showed, due to their smaller footprint, a rather high resistance compared to the bigger Ag/AgCl-electrodes made by NIKOMED (Nikotabs®, Nikomed, USA), we preferred the latter electrodes. The electrodes have been contacted using miniature crocodile clamps and unshielded wires with the length of 1m.

2.2. Electrode placement

Five healthy volunteers took place in the study, and their body impedance was repeatedly measured using different stimulation signals and measurement procedures. They were connected to the electrodes in a one-side arrangement with two electrodes (stimulus and monitor) at the left hand and the complementary electrodes at the left leg. The whole body was insulated to the ground with the exception of the unavoidable parasitic capacitances.

The distance between the stimulus and the monitor electrodes was 5 cm (Fig. 1). The probands rested for 10 min rest before the measurement started. Always ten measurements (1 measurement / s) were conducted for each experimental condition.



Figure 1. The driving electrodes 1 and 4 inject the stimulus while the monitor electrodes 2 and 3 monitor the voltage dropping across the body.

Using very fast measurement at a single frequency (100 measurements/s at 50 kHz), we proved a minimum sensitivity to heart activity and respiration during the measurements. However, despite the measurement is stable against vital body activities, moving artifacts still occur (Dunbar 1994). In order to cut out these artifacts, we calculated an average spectrum from the ten single measurements. All spectra which were outside a single standard deviation were removed, and the average spectrum was calculated again. In general, not more than one or two spectra per experiment were discarded. If electrode placement was bad or extreme movement artifact happened, we repeated the entire measurement.

2.3. Impedance measurement system

In spite of future developments, we took advantage of measurements in the time domain. The most critical part for this procedure is the choice of the excitation signal but also the sampling of the response. The suitable frequency range for BIA lies between 100 Hz and 1 MHz which is four orders of magnitude. Suitable broad bandwidth excitation signals are step functions, multi sine, maximum length sequence or chirp. All these functions are easily implemented in an arbitrary waveform generator. Throughout the experiments reported here, an AWG2021 (Tektronix, Beaverton, USA) was used for generation of the stimulating signal. The response was in all cases sampled by a DPO 2022B – oscilloscope (Tektronix). Both channels of the oscilloscope were used for measuring the voltage across the monitor electrodes and the total current injected. Since both waveforms, voltage and current may have slow edges (e.g., multi sine) or have a high noise level, we used the trigger output of the generator and the auxiliary trigger input of the oscilloscope for synchronization between generator and oscilloscope.

The analog frontend (Fig. 2) consisted of a differential driver which injected the stimulating waveform (voltage controlled) into the outer electrodes (most near to hand and leg, electrode 1 and electrode 4 at Fig. 1). The output voltage was set to 100 mV which resulted in steps of 200 mV due to the bipolar operation. The current was monitored as a voltage drop across a serial resistor. In order to guarantee symmetric operation, equal resistors were placed at each output of the driver (not shown). A high impedance, differential amplifier matched the signal to the 50 Ω impedance of the coaxial cable connecting the oscilloscope. An amplifier, equal to this for current measurement, was used for monitoring the voltage across the monitor electrodes. The input of the oscilloscope was terminated with a 50 Ω resistor.

The oscilloscope recorded the waveforms with 125.000 samples in 8-bit format (without average) or in 16-bit format (average). It should be noted that the 16-bit format does not necessarily mean that such resolution is indeed reached. This depends on the noise level of the signal and the number of averages (here 256).

The stimulus was applied as symmetrical repeating step functions (square wave) with voltage control at the electrodes 1 and 4 (Fig. 2). Due to the capacitive behavior of the skin and the electrodes, a differentiated signal appears as current. Therefore, the actual voltage across the inner electrodes is differentiated as well.

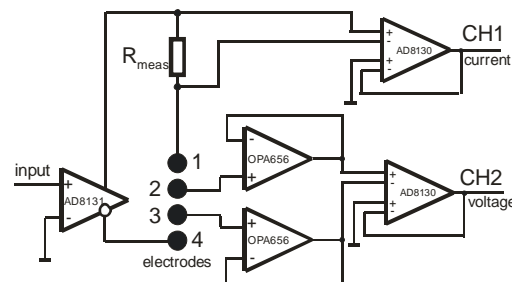


Figure 2. Schematic of the analog frontend: The stimulus is symmetrically driven, and the current and voltage monitors use equal circuitry (not completely shown).

The signals at electrode 1 and electrode 4 are equal but phase-shifted 180° (Fig. 3, A and B). Both the current through the body (Fig.3b) and the voltage across the monitor electrodes (Fig. 3D) are differentiated due to the capacitive behavior of the skin.

Attempts, to use current control showed considerable difficulties, especially for periods more than 1 ms. Since the electrodes and skin (especially stratum corneum) under the electrodes form a capacitor on the order of 10 nF (Fig. 4A), only a very small current can be applied, else the voltage across the electrodes reaches the supply voltage. Moreover, a dc-offset at the skin is always present and cannot be compensated. The use of higher frequency can circumvent some problems but comprises important information in the low-frequency region. The difficulties with the skin behavior and the electrode system become easier visible by looking at the equivalent circuit (Fig. 4). For a single electrode, the skin behavior under the electrode will overwhelm the electrical properties of the body (Fig. 4A). But not only the skin capacitance but also a Nernst-voltage (mostly at the stratum corneum) due to electrolytic imbalances within the skin can dramatically influence the measurements. The half-cell potentials of the electrodes are not considered here because they are approximately equal and canceled by the front end. Although not immediately clear, since the dc-part is well separated from ac, the dc-part can drive the

amplifiers into an unstable regime near the supply voltage. Blocking the dc-offset using a capacitor yields charge accumulation at this capacitor and increases the negative effect.

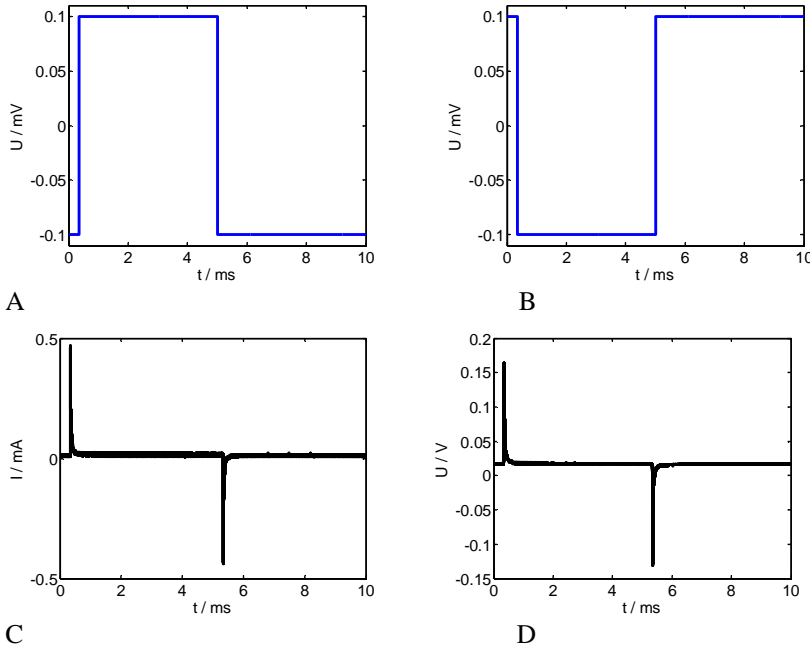


Figure 3. A symmetric signal applied at electrode 1 (A) and 4 (B), (C) current monitored across the sampling resistor and (D) voltage between the monitor electrodes 2 and 3.

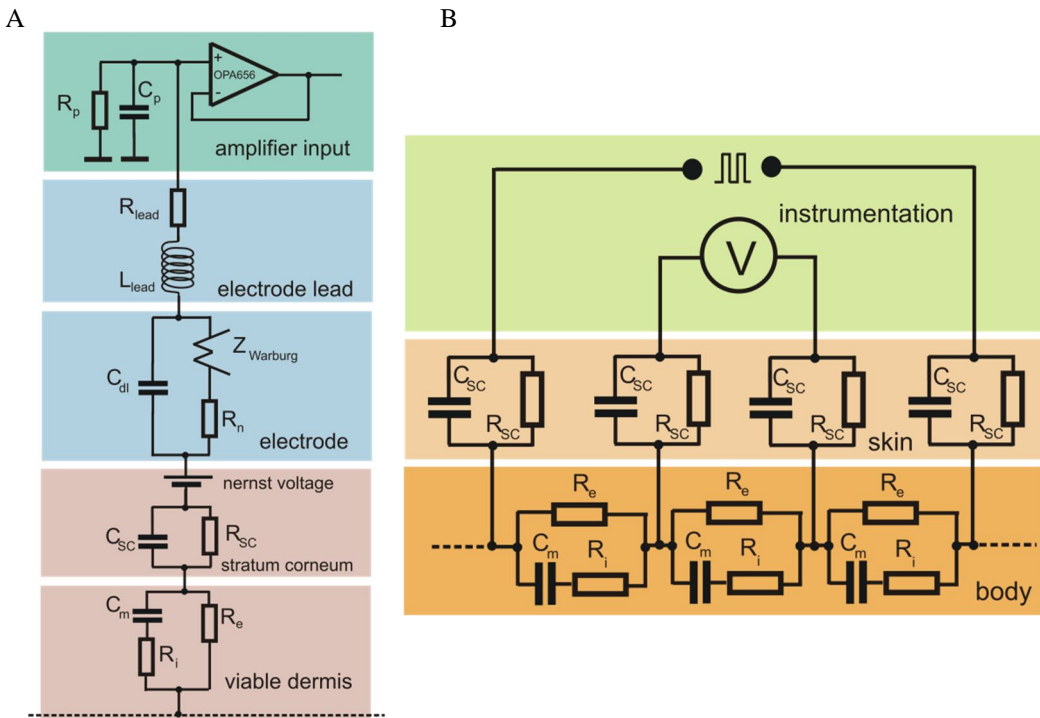


Figure 4. The impedance of the electrodes and the stratum corneum is highly problematic, especially for low-frequency measurements. A) equivalent circuit for one monitor electrode. Besides the electrode impedance (here modeled with Randles circuit) the skin impedance (capacitive behavior, galvanic resistance on the order of $100 \text{ k}\Omega\text{cm}^2$) a lead inductance and the parasitic input impedance of the amplifier needs to be considered. C_p, R_p – parallel parasitic capacity and resistance, $R_{\text{lead}}, L_{\text{lead}}$ – lead impedance (resistance and inductance), C_{dl} – double layer capacity, R_n – Nernst resistor due to charge exchange at the electrode, Z_{Warburg} – Warburg impedance, $C_{\text{sc}}, R_{\text{sc}}$ – capacity and resistance of the stratum corneum, C_m – lumped membrane capacitor, R_i – resistance of intracellular electrolytes, R_e – resistance of extracellular electrolytes. B) equivalent circuit for understanding the voltage across the monitor electrodes as well the total current through the body. No parasitic capacitance to earth is considered here.

Extending the equivalent circuit for all four electrodes shows clearly, that both current through the body and the voltage across the monitor electrodes is considerably influenced by parasitic elements. Besides passive elements, a Nernst voltage of about 200 mV is found due to the polarization at the epithelium (stratum corneum) under resting condition.

Compensation of the parasitic elements is not completely possible, but their influence is dramatically reduced by the front-end electronics and proper data processing. Moreover, limiting the frequency range and non-polarizing electrodes (Ag/AgCl) minimizes the influence of the Warburg impedance and inductive behavior of the 1meter long lead. The length of the leads arises from the usage of passive electrodes (without frontend electronics) and the placement of the electrodes.

2.4. Impedance matching

A critical point is the waveform of the signal in the high-frequency region, i.e., at the time when the step is applied. Care was taken that the step response of the amplifiers does not yield an overshoot or dc-falloff. This was accomplished by matching all cables from the generator to the device and back to the oscilloscope to 50 Ω . Since the oscilloscope did not have an internal termination, a 50 Ω through-resistor was used at each channel. The frontend output to the oscilloscope was terminated with a 50 Ω resistor in series. Since the low-frequency part is important, the oscilloscope was always dc-coupled.

2.5. Experimental uncertainties

Monitoring body electrical properties through high resistive skin remains a challenge. The magnitude of the body impedance was found, depending on frequency and individual between 100 Ω and 1 k Ω . Unfortunately, the skin resistance under the electrodes can be as high as several tens of k Ω in the low-frequency range. On the other hand, the capacity of the skin flap under the electrode is around 10 nF meaning that the arrangement electrode–skin has mostly capacitive behavior. The application of a controlled current is possible for higher frequencies or needs rather high voltage across the electrodes. At low frequency, even very low current on the order of some microampere can drive the output into the supply voltage.

During the experiments, electrodes may not be stable which is easily detectable. All experiments with misplaced or detached electrodes were discarded and repeated.

A high noise level due to building facilities like air conditioning or control systems appeared. Several attempts of grounding at different places gave only slight improvement of the signals. A significant improvement was reached by decreasing the current sampling resistors to 10 Ω .

The equipment, an arbitrary function generator, and a 2-channel oscilloscope needed exact synchronization which was accomplished by using the trigger-output of the function generator and the auxiliary trigger line of the oscilloscope. This prevented the uncertainty of slow edges or time shifts due to amplifiers or cabling in the measurement signal. In order to achieve the best results, the time base of the generator and oscilloscope were matched. Thus, exactly one period of the signal was measured. By using a step function, it is critical to assess the first μ s after but also before the step occurs. Therefore, the trigger point was set to 5 % (Fig. 3). The dynamic range of the oscilloscope was fully used by signal amplification to about 80 % of the screen. Both channels were placed in the middle of the screen.

Several tests have been made with multisine-signals, where also 100 Hz as fundamental frequency was used. These experiments served as a reference since this approach is better established than accessing the step response.

The reproducibility of the measurements was tested by 10 x measurements for every single experiment. Uncertainties in the high and low-frequency range were investigated in terms of the error propagation throughout the measurement chain. Especially the link between departures within the raw signal to the calculated impedance spectrum was under investigation and used for development of algorithms which can correct for systematic errors.

Care was taken for signal preprocessing by using the built-in anti-aliasing filter with a cutoff frequency of 1.4 MHz which is adequate for the bandwidth between 100 Hz and 1 MHz and a sample rate of 12.5 MS/s. The filter was only active in sample mode and was turned off during averaged acquisition. It should be noted that averaging itself has a filter function.

The aim of further measurements was to explore limitations for hardware and energy minimalizing. Especially we show that minimalized solutions with low data volume can achieve the same accuracy than reference methods using the full resources of the instrumentation.

Therefore, the response to step functions was traced using the oscilloscope, and further calculation (sample point, signal integration) was done digitally. Although this does not show any advantage for the

particular measurement, it is the basis for future developments, like for instance wearable systems with power harvesting.

A critical point in body impedance spectroscopy is the parasitic capacitance to ground. We tested several ways to couple the body on purpose either galvanically or capacitively to ground. Although, a shift in the spectrum was found, 'resonance like' points where the imaginary part becomes zero were not evident. If this appears, it is usually a result of poorly designed front ends.

For sensitivity assessment of the electrode configuration to moving artifacts and to body functions (respiration, heartbeat) measurements with high repetition rate (10 kHz) at a single frequency (50 kHz) were done. It turned out that the particular electrode configuration was almost insensitive to body functions but showed a great disturbance during body movements.

3. Data processing

3.1 Multisine as the reference measurement

The stimulus was continuously applied. This ensures steady state condition which is required for transformation into the frequency domain by fast Fourier transformation (reference measurements).

It is important that the time shift between current and voltage is essentially zero. This time shift depends mainly on the equipment used. The major disturbance was prevented by matching the group delay of the voltage and current channel. In our setup, the highest jitter between the channels was not more than the time between adjacent sample points, here 80 ns.

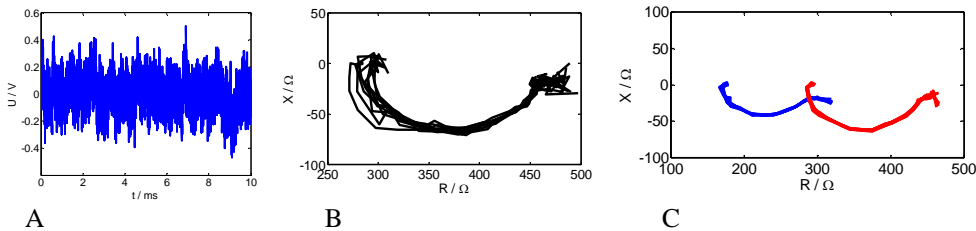


Figure 5. (A) Multisine signal used for excitation. (B) Wessels diagram from 10 single measurements with 1 s spacing and an electrode configuration shown in Fig. 1 without averaging of the current and voltage response (C) Wessels diagram, overlaid from two persons and ten single measurements but with 16 x averaging (blue male, red female).

Both voltage and current were transformed into frequency domain by fast Fourier transformation (FFT). Since the fundamental frequency of the excitation signal was set to 100 Hz and the horizontal deflection of the oscilloscope was 1 ms/s which results in 10 ms record time, exactly one period was transformed which is necessary for obtaining accurate results.

Using the recording in sample mode, only 8-bit resolution was available, and a higher noise level appeared. Therefore, the reproducibility of the measurements was less (Fig. 5 B) than with averaging (Fig 5.C). Having different probands, clear and reproducible differences in impedance, especially between male and female test persons, were found (Fig. 5.C).

3.2. Step response (relaxation behavior)

In general, the response of step function can be handled in the same way as the multisine response. In this sense, the step response does not show any advantage. Quite opposite, the noise level rises dramatically with increasing frequency due to the fast declining energy at higher harmonics.

In order to show the way for taking advantage of the step response with respect to energy minimization and minimal data volume, we use special processing where the first part until the sampled signal is under development as hardware solution (accompanying paper in this issue).

Sampling

The idea is to sample fast where fast changes of the signal occur and slow it down with time. Moreover, since we can assume that the signal is symmetrical between the half periods, only one half period needs to be sampled. With the sample vector obtained in this way, FFT is impossible and needs to be replaced by analytic integration of the product between the measured signal and test function (sine and cosine function). This implies that in opposite to FFT, the time point where the step is applied is 100% known and set to 0s. It would be simple by using hardware without any jitter. However, in our experiments a jitter of $\pm\Delta t$, which is for a sampling rate of 12.5 MS/s 80 ns was unavoidable (Fig. 6 A).

The exact time point t_0 of the step was calculated by means of the least square fit. Rounded to the next integer, it was used to extract exactly both half waves from the signal. Since the symmetry was proven, a mean of both half waves was calculated, resulting finally in only one half period. The time vector was adjusted with the fractional part of t_0 .

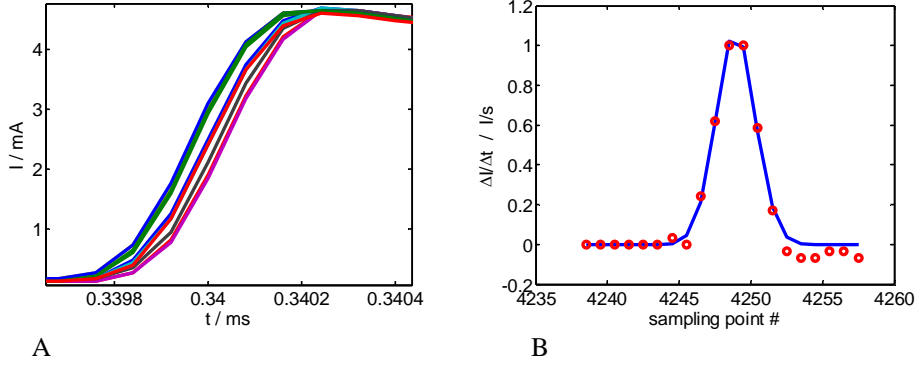


Figure 6. (A) The jitter of the trigger point for the current response. The uncertainty is about 160 ns. (B) Derivative of the current at the time when the step occurs (red circles). A nonlinear least-square fit was used for obtaining the exact, non-integer t_0 for further calculation.

Calculation of Fourier coefficients

It is essential by using discrete Fourier transformation that a complete period or a multiple of it is transformed. The coefficients are calculated as

$$c_k = \sum_{n=1}^N a_n e^{-j\omega_0 k} \quad ; k = 0, 1, 2, \dots, N-1; \quad \omega_0 = \frac{2\pi}{N} \quad (2)$$

It should be noted, that, compatible with the FFT in Matlab, c_1 is the dc-component and c_2 the coefficient for the fundamental frequency.

Looking closer at the behavior of signals with symmetrical half periods reveals that under strict circumstances, like no dc-offset, only one half wave is sufficient for transformation. In this case, the value of the coefficients, calculated separately for both half waves equals.

$$c_k^+ = \sum_{n=1}^{N/2} a_n e^{-j\omega_0 k} = c_k^- = \sum_{n=\frac{N}{2}+1}^N a_n e^{-j\omega_0 k} \quad (3)$$

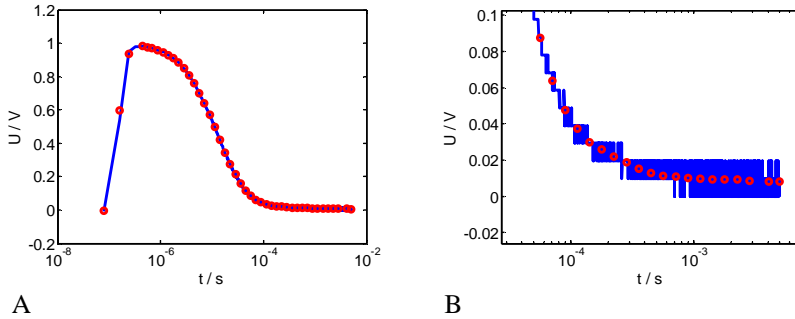


Figure 7. (A) Sampling points (red circles) for the voltage between the monitor electrodes. The logarithmic scale linearizes the time vector (logarithmic spacing) for better clarity. The voltage at each sampling point is calculated as the mean voltage between two time points. (B) is a zoom of the slow changing part of the signal sampled with 8-bit resolution.

It is essential for this condition that the dc-offset is zero because other than in ‘complete’ Fourier-transformation, a dc-offset influences all frequencies, not only the dc-component.

Since it is our intention to show ways for efficient hardware and data processing in the future (ultra-broad bandwidth, lowest energy consumption, minimal hardware), we resample the equidistantly spaced vector using a logarithmic function. Since simple sampling with increasing sample interval would violate the sampling theorem, adaptive low pass filtering was realized by integration over the entire sampling interval. This is a critical step, which is also required for future hardware solutions.

The re-sampled vector with logarithmic spacing cannot be transformed with established methods. The low number of samples (10/decade) allows a partial integration based on analytic solution between the sample points. Therefore, an analytic expression for the sample vector is required. A simple approach is the use of three adjacent points and an approximation of a square function

$$U(t_i) = at^2 + bt + c \quad (4)$$

Summing over the sample vector yields the complex Fourier coefficient for a particular frequency

$$A(\omega_k) = \sum_{i=2}^{N-1} \int_{t_{i-1}}^{t_{i+1}} (a_i t^2 + b_i t + c_i) e^{-j\omega_k t} dt \quad i = 2, 4, \dots, N-1 \quad (5)$$

The coefficients at the i^{th} sample point, a_i , b_i and c_i , are found as

$$\begin{aligned} a_i &= \frac{\frac{t_{i-1} - t_i}{t_{i-1} - t_{i+1}} (U_{i-1} - U_{i+1}) - (U_{i-1} - U_i)}{\frac{t_{i-1} - t_i}{t_{i-1} - t_{i+1}} (t_{i-1}^2 - t_{i+1}^2) - (t_{i-1}^2 - t_i^2)} \\ b_i &= \frac{(U_{i-1} - U_i) - a_i (t_{i-1}^2 - t_i^2)}{t_{i-1} - t_i} \\ c_i &= U_{i-1} - a_i t_{i-1}^2 - b_i t_{i-1} \end{aligned} \quad (6)$$

Now, the coefficients A_a and A_b can be calculated in an analytic way:

$$\begin{aligned} A_{a,k,i} &= \int_{t_{i-1}}^{t_{i+1}} (a_i t^2 + b_i t + c_i) \cos(k\omega_0 t) dt \\ &= \left[\frac{a[2k\omega_0 t \cos(k\omega_0 t) + (k^2\omega_0^2 t^2 - 2) \sin(k\omega_0 t)]}{(k\omega_0)^3} \right. \\ &\quad \left. + \frac{b[\cos(k\omega_0 t) + k\omega_0 t \sin(k\omega_0 t)]}{(k\omega_0)^2} + \frac{c \sin(k\omega_0 t)}{k\omega_0} \right]_{t_{i-1}}^{t_{i+1}} \end{aligned} \quad (7)$$

$$\begin{aligned} A_{b,k,i} &= \int_{t_{i-1}}^{t_{i+1}} (a_i t^2 + b_i t + c_i) \sin(k\omega_0 t) dt \\ &= \left[\frac{-a[2k\omega_0 t \sin(k\omega_0 t) - (k^2\omega_0^2 t^2 - 2) \cos(k\omega_0 t)]}{(k\omega_0)^3} \right. \\ &\quad \left. - \frac{b[\sin(k\omega_0 t) - k\omega_0 t \cos(k\omega_0 t)]}{(k\omega_0)^2} + \frac{c \cos(k\omega_0 t)}{k\omega_0} \right]_{t_{i-1}}^{t_{i+1}} \end{aligned} \quad (8)$$

The factor k stays for the number of the harmonic. Although any integer is possible, only odd numbers make sense, because, even numbers yield zero. We used a nearly logarithmic spacing of the frequency vector between 100 Hz and 1 MHz with ten frequencies per decade.

Although seemingly complicated, it is a pure analytical solution and needs minimal resources of an FPGA or microcontroller.

The voltage and current as function of frequency is:

$$U(j\omega) = 2(A_{U,a} + jA_{U,b}) \quad \text{and} \quad I(j\omega) = 2(A_{I,a} + jA_{I,b}) \quad (9)$$

A_a and A_b is the general result of the transformation. U or I depend on the input vector – voltage or current. The factor 2 arises from the transformation of only a half wave. We recall that this is only true for symmetric signals without dc-offset.

Finally, the transfer function is calculated by

$$Z(j\omega) = \frac{U(j\omega)}{I(j\omega)} \quad (10)$$

We note here that the use of independent electrodes for stimulus injection and voltage monitoring yields different sensitivity fields for current and voltage. For calculation of the impedance between the clamps, it is, however, essential to have equal sensitivity. Thus, only the transfer function but not the impedance is assessable. A typical result is presented in Fig.8.

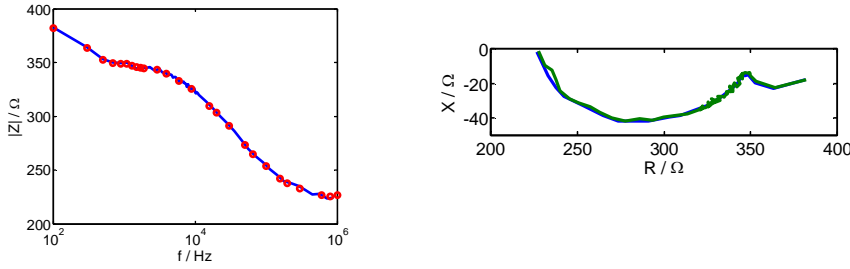


Figure 8. (A) The magnitude of the transfer function using the electrode configuration in Fig.1 for a healthy volunteer. The blue line is calculated a reference using ordinary FFT with logarithmic averaging of the unprocessed signal while the red circles show the result of data processing introduced above. (B) Wessel diagram for the same data in the comparison between both ways of processing.

A critical point for the applicability of a method is the reproducibility of the results but also the robustness against uncertainties in the measurement chain. Here, mostly timing errors and noise have been prominent sources of uncertainties. We repeated all measurements ten times with 1 s spacing (Fig.9). A high impact was found when the exact timing of the signals, especially the time when the step occurs (t_0) was not corrected.

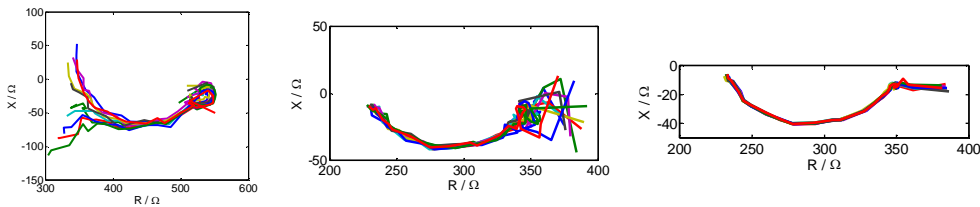


Figure 9. (A) Wessel diagram with ten subsequent measurements with 1 s spacing without processing of time vector and trigger condition, (B) corrected for jitter due to uncertain trigger. The data were filtered with a cutoff of 1.4 MHz and recorded without averaging. (C) measurements at the same test person but with 16x averaging and no filter applied.

The measurement uncertainty $F(Z)$ of the impedance measurement depends on both, the measurement method and the way of data processing. Moreover, at the high and low frequency, uncertainties are more prominent. In the low frequency region, mostly the high resistance of the electrodes overwhelms any influence from inside the body and at high frequency, cable effects and the

influence of parasitic capacitances, for instance between the body and ground become important. For comparison of measurement methods, we use the standard deviation of the complex impedance $s(Z)$ at each frequency with respect to its mean value \bar{Z} .

Table 1 gives averaged numbers for uncertainties found in our experiments with multisine and step excitation with and without averaging.

Table 1. Uncertainty for different methods calculated with ten independent measurements

f / Hz	multisine		step response	
	without average	average	without average	average
100	2.7402 + 0.1023i	1.7025 + 0.0714i	5.0607 + 0.2379i	0.5780 + 0.0226i
300	2.1958 + 0.0914i	0.4937 + 0.0129i	4.4360 + 0.0905i	0.5891 + 0.0244i
500	1.3108 + 0.0506i	0.6266 + 0.0193i	3.9387 + 0.1169i	0.5226 + 0.0186i
700	1.4755 + 0.0536i	0.6395 + 0.0227i	2.2014 + 0.1123i	0.3807 + 0.0149i
900	1.1611 + 0.0407i	0.5382 + 0.0199i	1.9239 + 0.1012i	0.3836 + 0.0169i
1100	1.0970 + 0.0426i	0.3901 + 0.0148i	2.1570 + 0.0950i	0.3127 + 0.0130i
1300	1.0109 + 0.0445i	0.2684 + 0.0105i	1.9406 + 0.0704i	0.2574 + 0.0095i
1500	1.1361 + 0.0515i	0.2096 + 0.0086i	1.5225 + 0.0479i	0.2391 + 0.0085i
1700	1.1412 + 0.0492i	0.2266 + 0.0097i	1.3443 + 0.0470i	0.2801 + 0.0110i
1900	0.9259 + 0.0372i	0.2502 + 0.0111i	1.6014 + 0.0648i	0.2880 + 0.0130i
2900	0.8501 + 0.0419i	0.2782 + 0.0138i	1.5547 + 0.0840i	0.2252 + 0.0122i
3900	0.6893 + 0.0442i	0.1920 + 0.0113i	1.0672 + 0.0692i	0.2313 + 0.0145i
5900	0.6450 + 0.0562i	0.1756 + 0.0136i	1.0654 + 0.0776i	0.2320 + 0.0180i
8900	0.5788 + 0.0611i	0.2479 + 0.0248i	0.6915 + 0.0679i	0.2741 + 0.0261i
15900	0.6756 + 0.0932i	0.2302 + 0.0298i	0.5564 + 0.0673i	0.2604 + 0.0313i
19900	0.7748 + 0.1155i	0.2400 + 0.0333i	0.5398 + 0.0663i	0.2840 + 0.0349i
29900	1.0621 + 0.1863i	0.1853 + 0.0309i	0.6380 + 0.0874i	0.2761 + 0.0374i
49900	1.1361 + 0.2040i	0.2078 + 0.0365i	0.7340 + 0.1064i	0.3100 + 0.0449i
65300	1.2263 + 0.2241i	0.1703 + 0.0285i	0.6326 + 0.0859i	0.3082 + 0.0425i
99900	1.5483 + 0.2685i	0.2444 + 0.0363i	0.9082 + 0.1162i	0.3322 + 0.0425i
157700	2.8160 + 0.4217i	0.4959 + 0.0656i	0.8064 + 0.0890i	0.2505 + 0.0279i
199900	3.6191 + 0.5022i	0.6457 + 0.0738i	1.0368 + 0.1058i	0.1740 + 0.0172i
299500	3.0593 + 0.2329i	0.3509 + 0.0249i	1.0567 + 0.0807i	0.3413 + 0.0256i
599900	3.9597 + 0.0676i	0.4132 + 0.0055i	1.1487 + 0.0642i	0.4567 + 0.0211i
799900	4.1149 - 0.0242i	0.5832 - 0.0022i	0.9889 + 0.0480i	0.4790 + 0.0194i
999900	3.4882 - 0.0106i	0.5719 - 0.0011i	0.9483 + 0.0378i	0.4526 + 0.0129i

4. Results and discussion

First, test measurements using multisine excitation were used for optimization of the equipment, especially the front end. Most important was the reduction of noise and drift behavior at the electrodes. Moreover, for noise reduction, we tested several ways of selective grounding which is justified when using symmetric excitation. If the grounding electrode is placed where the signal becomes zero, in this case in the region of the abdomen, no disturbance of the measurement is expected. Indeed, by monitoring the signal at the grounding electrode, small signal amplitude but not zero could be found. However, this did not reduce the noise level – in the opposite, sometimes we got even more noise. Under these circumstances, we discontinued these experiments and used complete insulation of the body.

The experiments have proven, that both the hardware and the data processing allows stable measurements. The electrodes remain critical. The bigger the electrodes, and therefore, the lower the resistance of the skin touching the electrodes, the better the results are.

Using the equations, derived by Cornish (Cornish 1996) for healthy persons, we calculated the total body water, and fat content of the volunteers taking place in this study (Fig.10). Although the right trend is clearly visible, inspecting the quantitative results makes the results questionable. The main reason is that the equations presented in many publications are specific for electrode placement, electrodes and the equipment used.

The direct comparison between excitation signals (Table 1) shows comparable uncertainties for the same hardware used. This is expected since the excitation signal should not influence the electrical properties of the object. However, it shows also clearly, that the often used argument that the energy of harmonics in step function declines with $1/f$ and therefore high noise level for high frequencies comprises the measurement result. This is not true if the data processing is done in the way shown here.

The procedure shown here becomes especially advantageous when high repetition or broad bandwidth measurements are required, and the data volume is a critical bottleneck as for instance in continuously scanning sensory fields. Moreover, with the sampling procedure burned in hardware, this approach allows extremely energy efficient applications of impedance measurement.

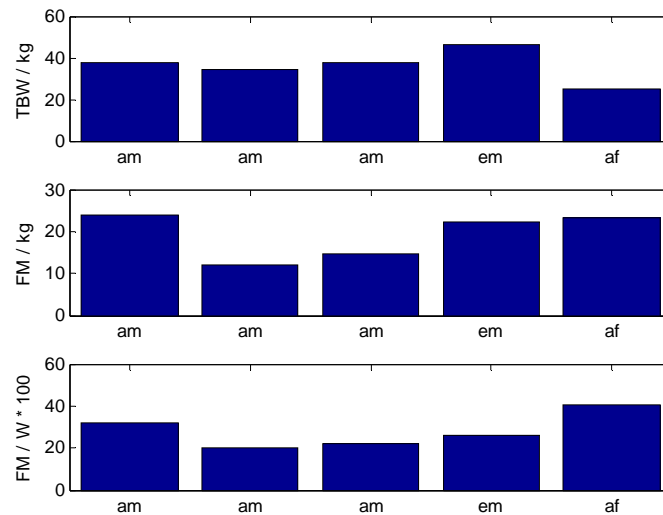


Figure 10. Total body water and fat content for the five volunteers in this study based on measurements of the impedance as described above. The indexes are *am* – Asian male, *af* – Asian female, *em* – European, male. Since the equations did only use the phase sensitive values of the impedance at 50 kHz, we derived this from the measurements.

5. Conclusion

Despite impedance measurements are long under investigation and are used for many applications, equipment for fast, broadband measurements with high repetition rate but ultralow power consumption are still missing. A concept, proven in this paper is the use of step functions for excitation together with adaptive sampling, aiming in nearly equally distributed energy throughout the spectrum for the sampled response. With timing as a hardware solution, this concept is feasible for ultralow power applications, such as a distributed system with energy harvesting.

Having only minimal data volume, the bottleneck of data transmission and processing becomes irrelevant.

6. Acknowledgment

This work was partially funded by a travel grant to UP by the Institute of Biomedical Physics, Ho Chi Minh City, and the Thüringer Aufbaubank (FKz 2016 FGR 0040).

7. References

- Bragos, R., Blanco-Enrich R., Casas, O., and Rosell, J. (2001) Characterisation of dynamic biologic systems using multisine based impedance spectroscopy, *Instrumentation and Measurement Technology*, 1, 44-47,
- Cornish, B. H., Ward, L. C., Thomas, B. J., Jebb, S. A., and Elia, M. (1996) Evaluation of multiple frequency bioelectrical impedance and Cole-Cole analysis for the assessment of body water volumes in healthy humans, *Eur. J. Clin. Nutr.* 50, 159-164
- de Lorenzo, A., Barra, P. F., Sasso, G. F., Battistini, N. C., and Deurenberg, P. (1991) Body impedance measurements during dialysis, *Eur. J. Clin. Nutr.* 45, 321-325

- Dunbar, C. C., Melahrinides, E., Michielli, D. W., and Kalinski, M. I. (1994) Effects of small errors in electrode placement on body composition assessment by bioelectrical impedance, *Res. Q. Exerc. Sport.* 65, 291-294
- Gabriel, S., Lau, R. W., and Gabriel, C. (1996) The dielectric properties of biological tissues: II. Measurements in the frequency range 10 Hz to 20 GHz, *Phys. Med. Biol.* 41, 2251-2269
- Hannan, W. J., Cowen, S. J., Plester, C. E., Fearon, K. C., and deBeau, A. (1995) Comparison of bio-impedance spectroscopy and multi-frequency bio-impedance analysis for the assessment of extracellular and total body water in surgical patients, *Clin. Sci. Colch.* 89, 651-658
- Lykken, D. T. (1971) Square-wave analysis of skin impedance, *Psychophysiology* 7, 262-275
- McAdams, E. T. and Jossinet, J. (1995) Tissue impedance: a historical overview, *Physiol. Meas.* 16, 1-13
- Min, M., Pliquett, U., Nacke, T., Barthel, A., Annus, P., and Land, R. (2008) Broadband excitation for short-time impedance spectroscopy, *Physiol Meas.* 29, 185-192
- Pliquett, U., Gersing, E., and Pliquett, F. (2000) Evaluation of fast timedomain based impedance measurements on biological tissue., *Biomed. Techn.*, 45, 6-13
- Schwan, H. P. (1957) Electrical Properties of Tissue and Cell Suspensions, In *Advances in Biological and Medical Physics*, 5, 147-209, New York, NY: Academic Press
- Schwan, H. P. (1993) Mechanisms responsible for electrical properties of tissues and cell suspensions, *Med. Prog. Technol.* 19, 163-165